IEEE Access
Multidisciplinary | Rapid Review | Open Access Journal

Received January 17, 2020, accepted February 24, 2020, date of publication March 2, 2020, date of current version March 12, 2020.

Digital Object Identifier 10.1109/ACCESS.2020.2977675

Enhancement of Heading Accuracy for GPS/INS by Employing Average Velocity in Low Dynamic Situations

MIN JUN CHOI, YONG HUN KIM, EUNG JU KIM, AND JIN WOO SONG, (Member, IEEE)
Department of Software Convergence, Sejong University, Seoul 05006, South Korea

Corresponding author: Jin Woo Song (jwsong@sejong.ac.kr)

This work was supported by the Ministry of Science and ICT (MSIT), South Korea through the Information Technology Research Center (ITRC) Support Program supervised by the Institute for Information & Communication Technology Promotion (IITP) under Grant IITP-2020-2018-0-01423, and in part by the Development of Automated Inspection System for Access Vulnerable Railway Facilities based on Unmanned Aerial Vehicle from the Unmanned Vehicle and SW Platform Research Program related to Public Procurement for Innovation funded by the Ministry of Land, Infrastructure and Transport (MOLIT) of Korean Government and Korea Agency for Infrastructure Technology Advancement (KAIA).

ABSTRACT In this paper, we proposed an algorithm that improves the heading accuracy of the global positioning system (GPS)/inertial navigation system (INS) integrated system used in automobiles by manipulating INS velocity and GPS velocity measurements. Two velocities are provided by the GPS receiver: the velocity calculated using the position difference and the velocity calculated using the Doppler shift. The velocity obtained using the position difference is an average velocity for a certain time period, which is inaccurate under dynamic conditions because of its time delay. In contrast, the velocity from the Doppler shift is an instantaneous velocity and has no time delay. However, it also relies on pseudo-range error and noise, which degrades the heading estimation accuracy in low dynamic situations. Thus, although the velocity measurements can improve heading accuracy, the navigation performance is often degraded when the velocity measurements are used for GPS/INS integration. To improve the heading accuracy by solving the aforementioned problems, we proposed a heading accuracy improvement algorithm that employs the average velocity measurements obtained using the averaged GPS velocity and the average velocity of the INS. Since the proposed average velocity measurements are calculated using long baseline, the proposed algorithm can improve the heading accuracy without using other sensors, especially in the case of low dynamic situations. It can be easily applied to the existing GPS/INS integrated system, making it suitable for use in automotive navigation systems. In this research, it is verified that the average velocity measurements can be substituted for Kalman filter measurements, and the performance improvements are confirmed through simulations and experiments.

INDEX TERMS Automobile vehicles navigation, GPS integrated navigation, velocity, heading accuracy, average velocity measurements.

I. INTRODUCTION

A global positioning system (GPS)/inertial navigation system (INS) integrated system is a navigation system mainly used in aircraft, ship, and military weapon systems requiring high accuracy and stability [1]–[4]. In recent years, autonomous platforms such as drones and autonomous vehicles have been commercialized, and GPS/INS integrated systems have been used in various platforms [5]–[9]. In the case of autonomous vehicles, level 2 or 3 automated driving systems out of the six autonomous driving levels presented in the National Highway Traffic Safety Administration were commercialized. The autonomous navigation systems in the second and third stages are only capable of auxiliary operation such as lane-keeping and departure alarm, obstacle detection, and emergency braking, and the driver's intervention is still necessary [10]. Route guidance and stability should be improved as well to reach the destination without operator intervention and advance to the

The associate editor coordinating the review of this manuscript and approving it for publication was Emre Koyuncu.

higher-level autonomy. To improve autonomous navigation without driver intervention, it is necessary to improve the accuracy of the navigation system.

Studies on the navigation systems for autonomous vehicles have mainly focused on improving the accuracy of navigation using new measurements and other additional sensors. GPS/INS and odometer/GPS/INS integrated systems have been studied [11]–[14]. Recently, studies have been conducted to improve the position accuracy using light detection and ranging (LIDAR) [15]–[18] or image sensors for map matching and road sign recognition [19]–[21]. The positioning based on precision map matching and the methods using LIDAR has the accuracy of less than several centimeters [17], and lane departure is detectable without other visual information when they are employed [18]. The above studies and methods of improving navigation accuracy using various sensors and devices require relatively expensive sensors and have a disadvantage in that they are likely to be degraded by environmental changes. Therefore, the GPS/INS integrated system is still essential for providing basic navigation information.

The existing low-cost GPS/INS integrated system, which is still indispensable to the automated driving system and is used as a fundamental navigation system, has the limitation of difficulty in the estimation of heading error and bias. To solve this problem, a system that integrates magnetic heading and GPS course or GPS velocity are usually designed. However, magnetic sensors are vulnerable to disturbances such as soft irons and hard irons, which limits performance improvement [22]–[24]. As the GPS course is different from the actual heading, they can be integrated only in vehicles with non-holonomic conditions or in special systems that require heading correction obtained using low-cost sensors [25]. In the case of automobiles, the GPS course can be used as the measurement because the non-holonomic constraint is employed. However, the reliability of the measurement cannot be secured because the accuracy of the GPS course is not guaranteed at low speed and vehicles tend to move at low speed in urban areas where accurate heading information is particularly required.

GPS velocity can be used as additional information more freely compared with GPS course or magnetic heading information. The calculation method of the GPS velocity is largely based on two different measurements: the GPS position and the Doppler shift. Although both methods fundamentally utilize the pseudo-range between the satellite and the receiver, they have different characteristics [26]–[28]. The velocity obtained from the GPS position difference is very sensitive to the position noise and baseline length, i.e., the position difference. Therefore, the noise is large in low dynamic cases because of short baseline length, and small at high dynamic cases. Furthermore, it indicates the average velocity during the period, so that high dynamic motion will induce delayed velocity information rather than the instant velocity at a certain time.

The velocity obtained from the Doppler shift is advantageous because the noise in low dynamic situations is smaller than the velocity from the position difference. Moreover, it is the instantaneous velocity because the Doppler information is directly used to calculate it. However, it is still difficult to ensure accuracy in the case of low dynamics because pseudo-range error and noise are also involved in the calculation of the velocity.

Although both velocities have insufficient accuracy in low dynamic situations, GPS velocity, especially that obtained from the Doppler shift, is widely used as measurement when it is difficult to estimate the velocity and heading owing to the low performance of the inertial measurement unit (IMU) [29], or when estimating the cornering stiffness of the side slip [30]. It is also used for the initial alignment of the GPS/INS integrated system [31]. Nevertheless, there are some limitations in using velocity measurements because of their inaccuracy in low dynamic situations.

In this paper, we propose a method to overcome the disadvantages of the GPS velocity measurement, which can cause time-delay and inaccuracy in low dynamic situations. The proposed method improves the heading accuracy by manipulating GPS velocity information and averaging it. By employing the average velocity concept and designating new velocity measurements, the proposed method reduces velocity noise and enhances the baseline length, which induces accurate heading results. The proposed algorithm can improve the heading accuracy more compared with the use of Doppler velocity, which is verified via simulations and experiments. Moreover, the proposed algorithm can be implemented more economically because it can be used with an existing outdated GPS receiver that does not provide velocity obtained using the Doppler shift.

The rest of this paper is organized as follows. Section II briefly explains the structure of a general GPS/INS integrated system, and the characteristics of the velocity integrated system are analyzed. We propose a new measurement method for the GPS average velocity and show that the new method is valid and effective in Section III. We also describe an algorithm that improves heading accuracy by using the new average velocity measurement. In Section IV, verified are the performance improvements through Monte-Carlo simulations and automobile experiments, and we conclude with some remarks.

II. GENERAL GPS/INS INTEGRATED SYSTEM

In a general GPS/INS integrated system, an extended Kalman filter (EKF) is used to estimate and compensate the position error, velocity error, attitude error, acceleration bias, and gyro bias using GPS position measurements [32], [33]. The error state variables of the EKF are generally given by

$$\delta x = \begin{bmatrix} \delta p^T & \delta v^T & \delta \phi^T & b_a^T & b_g^T \end{bmatrix}^T, \tag{1}$$

where $\delta p = \begin{bmatrix} \delta L & \delta l & \delta h \end{bmatrix}^T$ is the position error vector of the latitude, longitude, and altitude defined in the earth-centered,

earth-fixed coordinate system, $\delta v = \left[\delta v_N \ \delta v_E \ \delta v_D\right]^T$ is the instantaneous velocity error vector in the north-east-down (NED) frame, and $\delta\phi = \left[\delta\phi_N \ \delta\phi_E \ \delta\phi_D\right]^T$ is the attitude error vector in the NED coordinate system. $b_a = \left[b_{x,a} \ b_{y,a} \ b_{z,a}\right]^T$ and $b_g = \left[b_{x,g} \ b_{y,g} \ b_{z,g}\right]^T$ are the accelerometer bias vector and gyro bias vector, respectively.

The system model for the EKF with process noise w can be defined as

$$\delta\dot{x} = F\delta x + Gw. \tag{2}$$

Here, the system matrix F for the filter is defined by (3) to (11), as shown at the bottom of the next page, and G is defined as (12), as shown at the bottom of the next page. $\rho = \left[\rho_N \ \rho_E \ \rho_D\right]^T$ is the transport rate, and $\Omega = \left[\Omega_N \ \Omega_E \ \Omega_D\right]^T$ is the earth rotation angular velocity in the NED coordinate system. R_m and R_t are the meridian and traverse radii of curvature, respectively. R_{mm} and R_{tt} are values obtained by partially differentiating the meridian and traverse radii with latitude L respectively. $f = \left[f_N \ f_E \ f_D\right]^T = C_b^n f^b$ is the acceleration vector in the NED frame, and C_b^n is the rotation matrix from the body frame to the NED navigation frame. In this study, the acceleration bias and gyro bias are modeled as Markov processes by adding $\beta_a I_{3\times3}$ and $\beta_b I_{3\times3}$.

In general, the GPS/INS integrated system uses the position or both position and velocity provided by the GPS receiver as measurements. In the case of using the position as the measurement, the measurement model and the observation matrix H_1 is obtained as

$$\begin{aligned} z_1 &= H_1 x + v_1, \quad z_{m1} = p^I - p^G, \\ H_1 &= \left[I_{3\times3} \ O_{3\times12}\right], \end{aligned} \tag{13}$$

where v_1 is measurement noise modeled as white noise, and measurement z_{m1} is the difference between the INS position p^I and GPS position p^G. In the case of using the position and velocity as the measurements, the measurement model with white noise v_2 and the observation matrix H_2 becomes

$$\begin{aligned} z_2 &= H_2 x + v_2, \quad z_{m2} = \begin{bmatrix} p^I \\ v^I \end{bmatrix} - \begin{bmatrix} p^G \\ v^G \end{bmatrix}, \\ H_2 &= \begin{bmatrix} I_{3\times3} & O_{3\times3} & O_{3\times9} \\ O_{3\times3} & I_{3\times3} & O_{3\times9} \end{bmatrix}, \end{aligned} \tag{14}$$

where measurement z_{m2} additionally uses the difference between the INS velocity v^I and the GPS velocity v^G.

Although the measurement models defined in (13, 14) are widely used in various platforms, it is disadvantageous in that it is difficult to estimate the heading error and the corresponding gyro bias when low-cost sensors are used. To solve this problem, the non-holonomic characteristics of the vehicle are used, or the GPS velocity or GPS course measurements provided by the GPS receiver are used.

However, these approaches may cause erroneous results in specific situations. For example, in urban areas where vehicles move slowly, GPS velocity measurements and course measurements are prone to be inaccurate, which results in errors in the estimation of heading and the corresponding gyro bias. The non-holonomic constraint is also vulnerable in many cases. When a vehicle passes through a highway ramp, for example, the 2D non-holonomic condition is momentarily broken. Therefore, a method that can maintain the quality of the measurement even under low dynamic conditions is required. In this paper, we propose a modified algorithm to solve the problem by employing an average velocity concept and modifying velocity measurements instead of using the velocity measurement directly.

III. AVERAGE VELOCITY INTEGRATED GPS/INS NAVIGATION SYSTEM

A. CHARACTERISTICS OF GPS VELOCITY MEASUREMENT

Before we present the main idea of the proposed algorithm, the characteristics and limitations of GPS velocity measurements are analyzed first.

The velocity provided by low-cost GPS receivers used in loosely coupled GPS/INS integrated systems is typically computed using two methods: position differentials and Doppler shifts.

First, the velocity can be obtained by differentiating positions according to time. If p_k^G denotes the position in the NED frame obtained by a GPS receiver at the time t_k, a velocity $\bar{v}_k^G$ in the local navigation frame is calculated as

$$\bar{v}_k^G = \left[v_N \quad v_E \quad v_D\right]^T = \frac{p_k^G - p_{k-1}^G}{\Delta t}, \quad \Delta t = t_k - t_{k-1}. \tag{15}$$

The velocity calculated thus is not the instantaneous velocity but the average velocity during the sampling period Δt. Therefore, it may be different from the instantaneous velocity when a vehicle moves with high dynamics. Furthermore, the velocity error is directly related to the amount of position change and position error, so that slow movement of the vehicle causes large velocity error.

The second velocity calculation method uses the Doppler shift, which is caused by the relative velocity of the receiver to the GPS satellite [27], [28]. The Doppler shift D in GPS indicates the difference between the frequency d^s transmitted by the satellite and the frequency d^G received by the receiver as

$$D = d^G - d^s = -\frac{d^s}{c}[(v^s - v^G) \cdot S], \tag{16}$$

$$S = \frac{r^s - r^G}{\left\|r^s - r^G\right\|} = \left[S_x \quad S_y \quad S_z\right]^T, \tag{17}$$

where r^G and v^G are the position and velocity of the GPS receiver, respectively, and r^s and v^s are the position and velocity of the satellite, respectively. S is the line-of-sight vector from the satellite to the receiver. In (16), v^s, d^s, and the light speed c are known. Equation (16) can be rewritten as

$$(v^G \cdot S) = D + \frac{d^s}{c}\left(v^s \cdot S\right). \tag{18}$$

As the line-of-sight vector has noise, the velocity of the receiver can be obtained using the least-square method as

$$v_u = \left[\left(D + \frac{d^s}{c}\left(v^s \cdot S\right)\right) S^T \left(SS^T\right)^{-1}\right]^T. \tag{19}$$

Equation (19) indicates that the velocity of a receiver is closely related to the line-of-sight vector, which is also directly affected by the current receiver position error. In addition, as the Doppler shift measurement has relatively small signal-to-noise ratio when the vehicle is slow, the velocity obtained thus may cause a relatively large error in low dynamic cases.

B. AVERAGE VELOCITY MEASUREMENT

To improve the navigation performance by using the GPS velocity, measurement having less noise characteristic than

$$F = \begin{bmatrix} F_{11} & F_{12} & O_{3\times3} & O_{3\times3} & O_{3\times3} \\ F_{21} & F_{22} & F_{23} & C_b^n & O_{3\times3} \\ F_{31} & F_{32} & F_{33} & O_{3\times3} & -C_b^n \\ O_{3\times3} & O_{3\times3} & O_{3\times3} & -\beta_a I_{3\times3} & O_{3\times3} \\ O_{3\times3} & O_{3\times3} & O_{3\times3} & O_{3\times3} & -\beta_g I_{3\times3} \end{bmatrix}, \tag{3}$$

$$F_{11} = \begin{bmatrix} 0 & \dfrac{R_{mm}\rho_E}{R_m+h} & \dfrac{\rho_E}{R_m+h} \\ \dfrac{\rho_n}{\cos L}\left(\tan L - \dfrac{R_{tt}}{R_t+h}\right) & 0 & -\dfrac{\rho_N \sec L}{R_t+h} \\ 0 & 0 & 0 \end{bmatrix}, \tag{4}$$

$$F_{12} = \begin{bmatrix} \dfrac{1}{R_m+h} & 0 & 0 \\ 0 & \dfrac{\sec L}{R_t+h} & 0 \\ 0 & 0 & -1 \end{bmatrix}, \tag{5}$$

$$F_{21} = \begin{bmatrix} \dfrac{\rho_E R_{mm} v_D}{R_m+h} - \left(\rho_N \sec^2 L + 2\Omega_n\right) v_E - \rho_N \rho_D R_{tt} & 0 & \dfrac{\rho_E}{R_m+h} v_D - \rho_N \rho_D \\ \left(2\Omega_N + \rho_N \sec^2 L + \dfrac{\rho_D R_{tt}}{R_t+h}\right) v_N - \left(\dfrac{\rho_N R_{tt}}{R_t+h} - 2\Omega_D\right) v_D & 0 & \dfrac{\rho_D}{R_t+h} v_N - \dfrac{\rho_N}{R_t+h} v_D \\ \rho_N^2 R_{tt} + \rho_E^2 R_{mm} - 2\Omega_D v_E & 0 & \rho_N^2 + \rho_E^2 \end{bmatrix}, \tag{6}$$

$$F_{22} = \begin{bmatrix} \dfrac{v_D}{R_m+h} & 2\rho_D + 2\Omega_D & -\rho_E \\ -2\Omega_D - \rho_D & \dfrac{v_N \tan L + v_D}{R_t+h} & 2\Omega_N + \rho_N \\ 2\rho_E & -2\Omega_N - 2\rho_N & 0 \end{bmatrix}, \tag{7}$$

$$F_{23} = \begin{bmatrix} 0 & -f_D & f_E \\ f_D & 0 & -f_N \\ -f_E & f_N & 0 \end{bmatrix}, \tag{8}$$

$$F_{31} = \begin{bmatrix} \Omega_D - \dfrac{\rho_N}{R_t+h} & 0 & \dfrac{\rho_N}{R_t+h} \\ -\dfrac{\rho_E R_{mm}}{R_m+h} & 0 & -\dfrac{\rho_E}{R_m+h} \\ -\Omega_N - \rho_N \sec^2 L - \dfrac{\rho_D R_{tt}}{R_t+h} & 0 & -\dfrac{\rho_D}{R_t+h} \end{bmatrix}, \tag{9}$$

$$F_{32} = \begin{bmatrix} 0 & \dfrac{1}{R_t+h} & 0 \\ -\dfrac{1}{R_m+h} & 0 & 0 \\ 0 & -\dfrac{\tan L}{R_t+h} & 0 \end{bmatrix}, \tag{10}$$

$$F_{33} = \begin{bmatrix} 0 & \Omega_D + \rho_D & -\rho_E \\ -\Omega_D - \rho_D & 0 & \Omega_N + \rho_N \\ \rho_E & -\Omega_N - \rho_N & 0 \end{bmatrix}, \tag{11}$$

$$G = \begin{bmatrix} O_{3\times3} & O_{3\times3} & O_{3\times3} & O_{3\times3} & O_{3\times3} \\ O_{3\times3} & C_b^n & O_{3\times3} & O_{3\times3} & O_{3\times3} \\ O_{3\times3} & O_{3\times3} & -C_b^n & O_{3\times3} & O_{3\times3} \\ O_{3\times3} & O_{3\times3} & O_{3\times3} & I_{3\times3} & O_{3\times3} \\ O_{3\times3} & O_{3\times3} & O_{3\times3} & O_{3\times3} & I_{3\times3} \end{bmatrix} \tag{12}$$

the conventional velocity measurement is required. Therefore, in this study, we modify velocity measurement by designating a new measurement with relatively small noise and long baseline.

For measurement with low noise, an average velocity concept is proposed in this paper. To apply the concept, it must be verified first whether the instantaneous velocity measurement can be replaced with the average velocity measurement for a short time without loss of generality. In this paper, it is proposed that the average velocity can be used instead of instantaneous velocity in low dynamic situations. The low dynamic situations are categorized into two cases: accelerated motion without rotational motion and constant rotational motion without acceleration.

As the effect of the earth rotation rate and other related terms can be ignored for a short time period, the attitude error, velocity error, and rotation matrix can be simplified as [33]

$$\begin{aligned}\delta\dot{\phi} &= -C_b^n b_g,\\ \delta\dot{v} &= C_b^n\left[\left(f^b\times\right)\delta\phi + b_a\right],\\ \dot{C}_b^n &= C_b^n\Omega_b,\end{aligned} \tag{20}$$

where $\omega_x, \omega_y, \omega_z$ are rotation rates along the x-, y-, and z-axes, respectively, and rotation rate in the body frame Ω_b and acceleration in the body frame $\left[f^b\times\right]$ can be defined as

$$\Omega_b = \begin{bmatrix} 0 & -\omega_z & \omega_y \\ \omega_z & 0 & -\omega_x \\ -\omega_y & \omega_x & 0 \end{bmatrix}, \tag{21}$$

$$\left[f^b\times\right] = \begin{bmatrix} 0 & -f_z & f_y \\ f_z & 0 & -f_x \\ -f_y & f_x & 0 \end{bmatrix}. \tag{22}$$

When a Kalman filter is employed at time t_k, the velocity error and the attitude error at $t_k + t$ can be expressed as a function of input acceleration, attitude, residual attitude error $\delta\phi(t_k)$, residual accelerometer bias $b_a(t_k)$, and residual gyro bias $b_g(t_k)$ after error correction. Further, the attitude can be obtained as

$$C_b^n(t_k+t) = C_b^n(t_k)\exp\int_{t_k}^{t_k+t}\Omega_b(\tau)\,d\tau. \tag{23}$$

Assuming that a vehicle moves gradually with low dynamics for a short time, the angular rate is supposed not to change significantly. In addition, ω_x and ω_y are supposed to be zero, and ω_z will be small. In this case, we can model the rate as

$$\Omega_b(t_k+t) = \Omega_{b,0} + \Omega_{b,v}(t_k+t), \tag{24}$$

where $\Omega_{b,0}$ is a constant rate during t_k to $t_k + t$, and $\Omega_{b,v}(t)$ is a random rate owing to the road condition or other external disturbances, whose average value will be zero.

From (24), (23) can be rewritten as

$$\begin{aligned}&C_b^n(t_k+t)\\ &= C_b^n(t_k)\exp\int_{t_k}^{t_k+t}\left(\Omega_{b,0}+\Omega_{b,v}(\tau)\right)d\tau\\ &= C_b^n(t_k)\exp\left(\Omega_{b,0}t + \int_{t_k}^{t_k+t}\Omega_{b,v}(\tau)\,d\tau\right)\\ &= C_b^n(t_k)\exp\left(\Omega_{b,0}t\right)\\ &= C_b^n(t_k)\left(I + \Omega_{b,0}t + \frac{1}{2}\Omega_{b,0}^2t^2 + \frac{1}{6}\Omega_{b,0}^3t^3 + \ldots\right)\\ &= C_b^n(t_k)\left(I + \Omega_{b,0}t + \frac{1}{2}\Omega_{b,0}^2t^2 + H\cdot O\cdot T(t)\right)\\ &\cong C_b^n(t_k)\left(I + \Omega_{b,0}t + \frac{1}{2}\Omega_{b,0}^2t^2\right).\end{aligned} \tag{25}$$

As $\Omega_{b,0}$ is small and ω_x and ω_y are assumed to be zero, $\Omega_{b,0}$ can be approximated as

$$\Omega_{b,0}\cong\begin{bmatrix} 0 & -\omega_z & 0 \\ \omega_z & 0 & 0 \\ 0 & 0 & 0 \end{bmatrix}, \tag{26}$$

and the higher order term in (25) can be ignored because of small t and small ω_z. For example, when t is 0.1 seconds and ω_z is 15°/s (0.26 rad/s), the second order term $\frac{1}{2}\Omega_{b,0}^2t^2$ becomes 3.38×10^{-3}, and the higher order term $\frac{1}{6}\Omega_{b,0}^3t^3$ is 2.93×10^{-6}, which is less than 0.1% of the second order term. Therefore, the higher-order term is ignored and extended to the second term for accurate calculation.

From (25) and (26), (20) can be solved as

$$\begin{aligned}&\delta\phi(t_k+t)\\ &= \delta\phi(t_k) - C_b^n(t_k)\left(I\cdot t + \frac{1}{2}\Omega_{b,0}t^2 + \frac{1}{6}\Omega_{b,0}^2t^3\right)b_g(t_k).\end{aligned} \tag{27}$$

The residual gyro bias $b_g(t_k)$ is constant during a short time period, and can be approximated as

$$b_g(t_k)\cong\left[\,0\;0\;b_{z,g}(t_k)\,\right]^T, \tag{28}$$

because roll and pitch gyro biases are observable enough to be compensated completely.

From (26) and (28), $\Omega_{b,0}b_g(t_k) = O_{3\times1}$. Therefore, (27) can be simplified as

$$\begin{aligned}&\delta\phi(t_k+t)\\ &= \delta\phi(t_k) - C_b^n(t_k)\left(b_g(t_k)t + \frac{1}{2}\Omega_{b,0}b_g(t_k)t^2\right.\\ &\quad\left. + \frac{1}{6}\Omega_{b,0}^2b_g(t_k)t^3\right)\\ &= \delta\phi(t_k) - C_b^n(t_k)b_g(t_k)t.\end{aligned} \tag{29}$$

After Kalman filter update, we have

$$\delta\dot{v}(t_k+t) = C_b^n(t_k+t)\left[\left(f^b\times\right)\delta\phi(t_k+t) + b_a(t_k)\right]. \tag{30}$$

We can also assume that the acceleration f^b during a short time period is mainly constant because the acceleration applied to a car is caused by the driver's reaction such as hitting pedals and it induces an acceleration or deceleration force. Even when a car makes a turn, it will mainly experience constant centrifugal acceleration.

In a low dynamic situation when a vehicle moves straight without rotational motion, $C_b^n(t_k+t)$ for a short time becomes constant i.e., $C_b^n(t_k)$. Therefore, from (29), (30) becomes

$$\begin{aligned}&\delta\dot{v}(t_k+t)\\&=C_b^n(t_k)[(f^b\times)(\delta\phi(t_k)-C_b^n(t_k)b_g(t_k)t)+b_a(t_k)]\\&=C_b^n(t_k)(f^b\times)\delta\phi(t_k)-(C_b^n(t_k))^2b_g(t_k)t+C_b^n(t_k)b_a(t_k).\end{aligned}\tag{31}$$

Here, the first and third terms are constant, and the second term increases in proportion to time.

In a low dynamic situation when a vehicle rotates slowly and steadily with small acceleration, it is assumed that $f^b \cong \begin{bmatrix}0 & 0 & f_z\end{bmatrix}^T$ for a short time and $C_b^n(t_k+t) \cong C_b^n(t_k)\left(I+\Omega_{b,0}t+\frac{1}{2}\Omega_{b,0}^2t^2\right)$. In addition, the roll and pitch errors become smaller than the yaw error because no acceleration is applied along their axes, which indicates that $\delta\phi(t_k) \cong \begin{bmatrix}0 & 0 & \delta\phi_D(t_k)\end{bmatrix}^T$. Therefore, we have

$$\left(f^b\times\right)\delta\phi(t_k)=O_{3\times1},\tag{32}$$

From (32), (30) can be written as

$$\begin{aligned}&\delta\dot{v}(t_k+t)\\&=C_b^n(t_k+t)\left(f^b\times\right)\delta\phi(t_k)-C_b^n(t_k+t)C_b^n(t_k)b_g(t_k)t\\&\quad+C_b^n(t_k+t)b_a(t_k)\\&\cong C_b^n(t_k+t)C_b^n(t_k)b_g(t_k)t+C_b^n(t_k+t)b_a(t_k)\\&=C_b^n(t_k)\left[-\left(I+\Omega_{b,0}t+\frac{1}{2}\Omega_{b,0}^2t^2\right)C_b^n(t_k)b_g(t_k)t\right.\\&\quad\left.+\left(I+\Omega_{b,0}t+\frac{1}{2}\Omega_{b,0}^2t^2\right)b_a(t_k)\right].\end{aligned}\tag{33}$$

Here, the first term in the parentheses is constant, and the second term is mainly proportional to time. The third term is mainly constant and partially proportional to time.

From (31) and (33), we can conclude that the velocity change in a low dynamic situation is affected by the attitude error, gyro bias, and accelerometer bias, differently. When the attitude error is involved, the velocity error is constant, and for the gyro bias, the velocity error is mainly proportional to time. When the accelerometer bias is involved, the velocity change is mainly constant as well.

Therefore, we can conclude that the velocity error, at a short period after the measurement update of Kalman filter, is mainly governed by the residual velocity error, residual attitude error, residual gyro bias, and residual accelerometer bias.

To analyze their influences on the velocity error, assume that the initial acceleration bias is 3 mg, and the initial gyro bias is 0.028°/s (100°/h). As residuals after the Kalman filter measurement update are usually less than 1%, the roll and pitch error of a conventional GPS/INS is less than 0.1° (0.0017 rad), and the yaw error is less than 0.5° (0.0087 rad) in a low dynamic situation, the velocity errors owing to residual errors can be obtained by integrating (31) and (33) as shown in Table 1 when we assume that a vehicle moves in the north direction initially.

TABLE 1. Velocity error owing to residual error.

	Residual error	Maximum north directional velocity error
Attitude error	0.0017/0.0087 rad (roll, pitch/yaw)	$0.0158\,t$
Gyro bias	4.89×10^{-6} rad/s (0.00028°/s)	$0.0000244t^2$ $+0.000000285t^3$ $+0.0000000186t^4$
Acceleration bias	2.94×10^{-4} m/s^2 (0.03 mg)	$0.000294t$ $+0.0000257t^2$ $+0.00000149t^3$

The results show that the instantaneous velocity errors owing to the acceleration bias and gyro bias are approximately 1.86% and 0.15% of the error owing to the attitude error, respectively. Therefore, the instantaneous velocity error is mostly affected by the residual attitude error, followed by the accelerometer bias, rather than the residual gyro bias. Noting that the velocity error increases in proportion to time according to the residual attitude error and accelerometer bias, it can be assumed that the instantaneous velocity error is mainly proportional to t in a low dynamic situation, which indicates that the instantaneous velocity measurement can be replaced with the average velocity measurement.

When we use the average velocity measurement instead of instantaneous velocity, the noise characteristics of the measurement will be changed. For the GPS velocity V_k^{G} with white Gaussian noise $v_k \sim N(0,R)$ at time t_k as shown in

$$V_k^{\mathrm{G}}=v_k^G+v_k,\tag{34}$$

the average velocity for the averaging period αT^G (α is a positive integer and T^G is the GPS sampling period) becomes

$$\bar{V}_k^{\mathrm{G}}=\frac{1}{\alpha}\sum\nolimits_{i=k-\alpha+1}^{k}\left(v_i^G+v_i\right)=\bar{v}_k^G+\bar{v}_k.\tag{35}$$

Here, the averaged noise $\bar{v}_k$ becomes white Gaussian noise as

$$\bar{v}_k \sim N\left(0,\frac{1}{\alpha}R\right),\tag{36}$$

because the noises at every time are uncorrelated. Equation (36) indicates that the averaged GPS velocity has smaller measurement noise than instantaneous GPS velocity, which results in enhancement of measurement quality. In addition, as the average velocity is vector information with a longer baseline, the direction angle information in the measurement is more useful and is relatively accurate. The baseline length of the average velocity is the product of the averaging time T and the average velocity $\bar{V}$. In the case of instantaneous velocity, it can be assumed that there is no baseline. The longer baseline contributes to the enhancement of heading estimation because the measurements with longer baseline can provide more accurate direction information than those with shorter baseline even though they have the same noise

characteristics. By averaging GPS velocity and INS velocity, the noise can be reduced in both cases and heading information can be more effectively extracted from the averaged velocity information. By using the average velocity with the above advantages, therefore, the accuracy of the heading can be improved.

C. HEADING ACCURACY ENHANCEMENT ALGORITHM

In this study, we improve the heading accuracy by utilizing the average velocity. We propose an algorithm that uses the average velocity as measurement. Fig. 1 shows the structure of the proposed heading accuracy enhancement algorithm. In the proposed algorithm, the average velocity is used for measurement update instead of the instantaneous velocity. As the algorithm is more valid in a low dynamic situation, the measurements are qualified and selectively chosen between the average velocity and instantaneous velocity. The additional part in the proposed algorithm is restrained, so that it can be applied to an existing integrated navigation system simply.

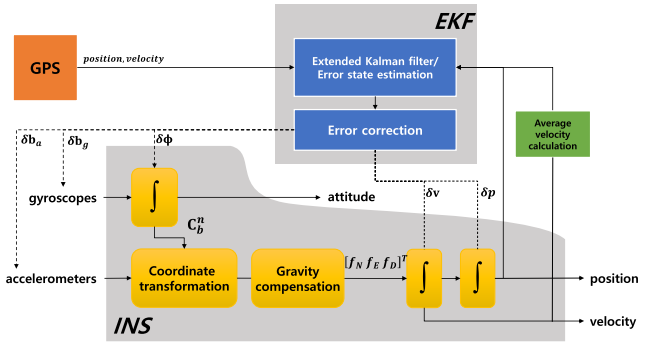

FIGURE 1. Block diagram of the heading accuracy enhancement algorithm.

The EKF error model used in the heading accuracy enhancement algorithm is the same as the model F in (2). As the measurement model uses the average velocity as a measurement, the measurement matrix of (37) and the observation matrix of (38) are used instead of the existing measurement model.

$$z = Hx + v, \quad z_m = \begin{bmatrix} p_k^I \\ \bar{v}_k^I \end{bmatrix} - \begin{bmatrix} p_k^G \\ \bar{V}_k^G \end{bmatrix}, \tag{37}$$

$$H = \begin{bmatrix} I_{3\times3} & O_{3\times3} & O_{3\times9} \\ O_{3\times3} & I_{3\times3} & O_{3\times9} \end{bmatrix}. \tag{38}$$

As the average velocity of GPS is used as the measurement, the average velocity $\bar{v}_k^I$ of INS should be calculated by using the instantaneous velocity v_k^I of INS. The average time αT^G is selected adaptively according to the dynamic condition. When the moving speed is very low, α can be set larger. In general, $\alpha = 2$ to account for not only low dynamic situations but also medium dynamic situations.

D. VALIDATION OF THE PROPOSED ALGORITHM USING SIMULATIONS UNDER VARIOUS DYNAMIC SITUATIONS

To validate the proposed algorithm, some simulations under various dynamic situations were conducted. In the simulations, the proposed algorithm is compared with the conventional algorithms, i.e., 1) algorithm that uses GPS position measurement only, 2) algorithm that uses GPS position and velocity based on position differences, and 3) algorithm that uses GPS position and Doppler velocity as measurements. The simulated dynamic conditions are varied by employing different speeds and accelerations as shown in Table 2. The simulation trajectory is shown in Fig. 2.

TABLE 2. Heading RMSE according to driving speed.

	Position-Only	Position+ V_{diff}	Position+ V_{dopp}	Proposed algorithm
Below 10 km/h	1.0412	1.0812	0.2991	0.2569
10–50 km/h	0.2868	2.8512	0.2375	0.1968
Over 50 km/h	0.2569	1.5892	0.1627	0.1709

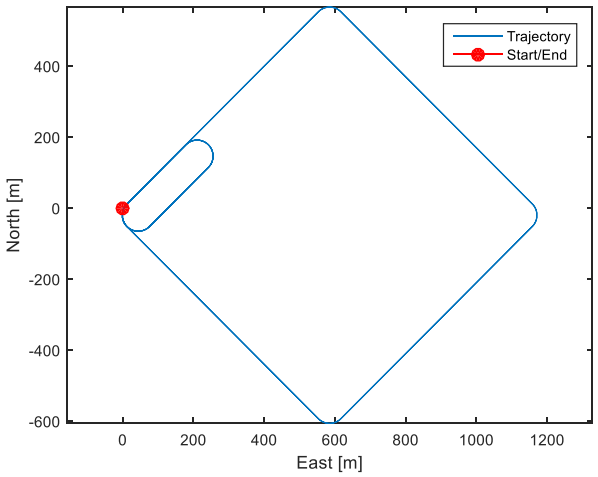

FIGURE 2. Simulation path according to speed.

The IMU used in the simulation is assumed to be a low-grade IMU with gyro bias of 0.5°/s and acceleration bias of 35 mg after initial calibration. The accuracy of GPS position is assumed to be less than 3 m circular error probability (CEP) and accuracy of GPS velocity is set to 0.1 m/s (RMS, root-mean-square). To evaluate the performance of heading error estimation, the initial heading error is set to 3°. The error model for EKF used in the simulation is the same as the model described in Section II, and the algorithm for improving the heading accuracy is the same as that described in Section III.C.

For accurate analysis, Monte Carlo simulations were performed 200 times and the root-mean-square errors (RMSE) were calculated after the Kalman filter converges. Table 2 shows the RMSE of heading for each dynamic situation.

Position-only results represent a conventional GPS/INS navigation that uses GPS position only as a measurement. In the case of position+V_{diff}, the position and the velocity obtained using the GPS position difference are used as measurements. Position+V_{dopp} indicates the case in which the position and Doppler velocity V_{dopp}, are used as measurements. The proposed algorithm uses the heading accuracy enhancement algorithm presented in Section III.C.

In the case of position+V_{diff}, the heading RMSE is the largest in all three driving conditions, compared with the case of position-only. This is because the quality of the measured value is poor because of the time delay error in V_{diff}. Therefore, V_{diff} information is not suitable for a measurement except in special cases.

In the case of position+V_{dopp}, the heading RMSE is lower than that of position-only. This is because the velocity, which is more directly related to the heading accuracy, is used as the measurement rather than the position. However, the actual Doppler velocity is contaminated by noise at very low speed, which results in insufficient performance improvement than expected. In the case of high speed, the baseline is lengthened, which contributes to the decrease of heading error even in the case of position-only.

In the proposed algorithm, the heading RMSE is lower than that of position+V_{dopp} in the various driving conditions. It has been shown that the proposed algorithm can enhance the measurement quality and compensate for the limitation of the existing GPS velocity by utilizing the advantage of the average velocity. When a vehicle moves at the speed of below 50 km/h, the proposed algorithm can take full advantage of long baseline and low noise measurements. At the speed of 50 km/h and above, the heading RMSE is slightly larger than that in position+V_{dopp}. This is because of the long baseline effect outweighs other advantages. However, as the error is only approximately 5% larger, we can confirm that the proposed algorithm at high speed has a similar heading accuracy to the case of using V_{dopp} as a measurement.

Fig. 3 shows the heading errors of the simulation results according to the speed. It also shows that the result of the proposed algorithm is superior to the other results as shown by the results in Table 2. In the case of position+V_{diff}, since the time delay error increases in the rotation section, the direction angle error increases excessively.

In these simulations, it was confirmed that the proposed algorithm can improve the heading accuracy in low dynamic situations by compensating the disadvantage of GPS velocity, which has large noise at low speed. In the next section, we will verify the proposed algorithm using the simulations for the compound driving route.

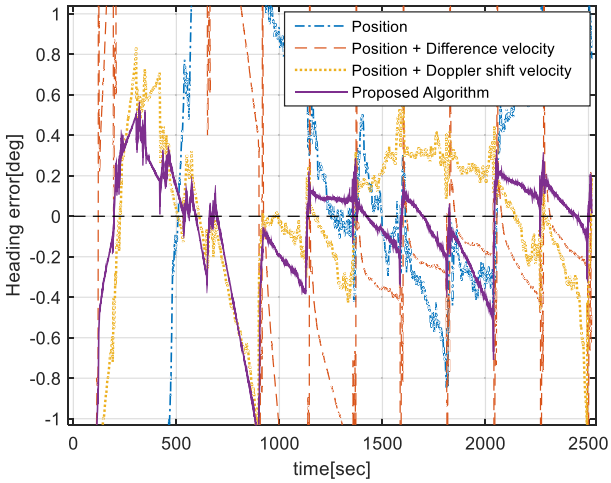

A. Driving condition 10km/h or less

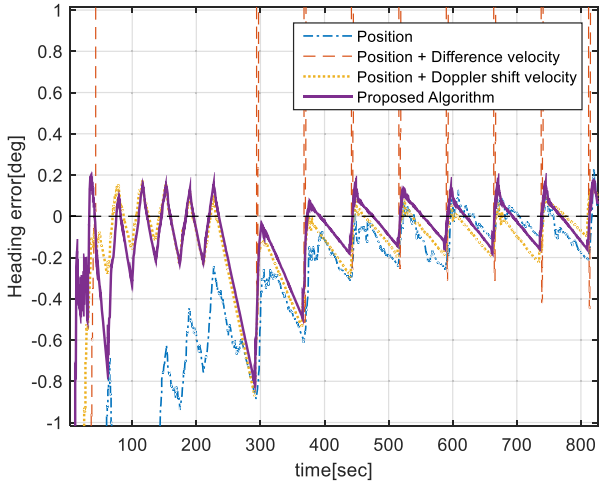

B. Driving condition 10~50km/h

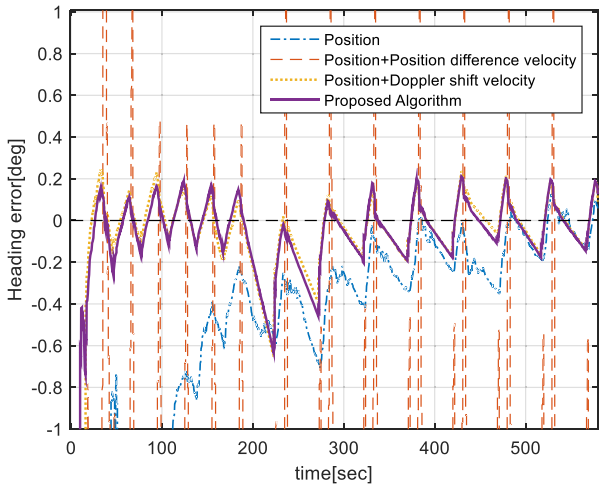

C. Driving condition 50km/h or more

FIGURE 3. Heading error according to driving condition.

IV. PERFORMANCE VERIFICATION

A. MONTE CARLO SIMULATION RESULTS

To verify the proposed algorithm under the various driving environments, Monte Carlo simulations were performed for the compound driving route shown in Fig. 4.

The high dynamic driving conditions and low dynamic conditions are simulated thoroughly. The speed varies from 0 km/h to 80 km/h. As the automobile turns, it decelerates

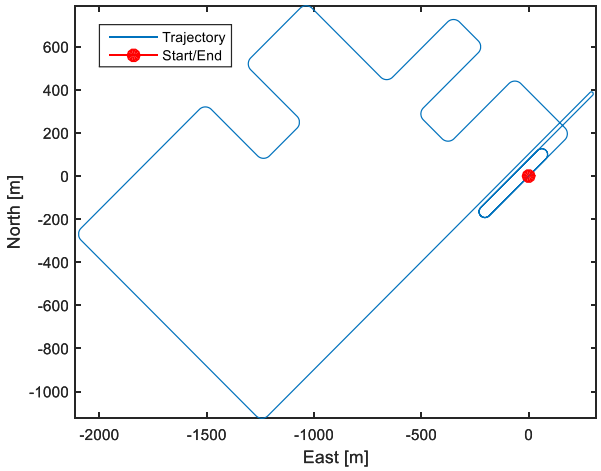

FIGURE 4. Combination driving route for Monte Carlo simulations.

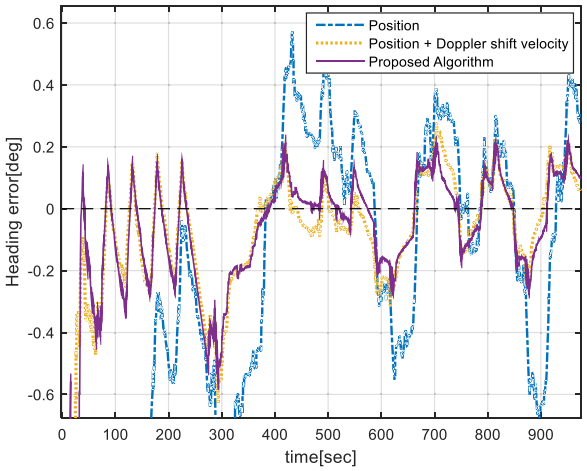

FIGURE 5. Heading error in the compound driving simulations.

TABLE 3. Heading RMSE in compound driving simulation.

	Position-only	Position + V_{dopp}	Proposed algorithm
Heading RMSE (deg)	0.3131	0.1862	0.1481

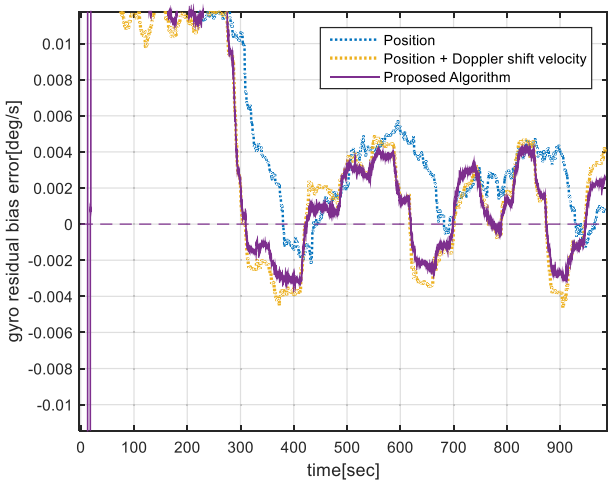

FIGURE 6. Residual z-axis gyro bias error in the compound driving simulations.

to less than 30 km/h and accelerates again. The IMU is assumed to be a low-grade IMU with gyro bias of 0.5°/s and accelerometer bias of 35 mg before initial calibration. The accuracy of GPS position is assumed to be 3 m (CEP) and the accuracy of GPS velocity is set to 0.1 m/s (RMS).

To compare the results, Monte Carlo simulations of 300 times were performed for three cases mentioned in section III-D. To evaluate the performance of heading estimation, the initial heading error is set to 3°. The RMSE error was calculated after the filter converges, and Table 3 shows the RMSEs of the results for three cases.

When the case of position+V_{dopp} is compared with the position-only case, the heading RMSE is considerably reduced because the velocity measurements have a more direct influence on the heading quality than the GPS position measurements.

In the case of using the proposed algorithm, it can be observed that the heading RMSE is reduced more dramatically than in the case of position+V_{dopp}. The proposed algorithm improves the heading accuracy by using long baseline vector information with smaller noise, which are the advantages of average speed even in a compound driving environment.

Fig. 5 presents the average heading error of Monte Carlo simulations. It can be observed that the heading error of the proposed algorithm is smaller than that in the position+V_{dopp} and position-only cases. Fig. 6 shows the gyro bias estimation performances. The results show that the estimation error for the z-axis gyro bias is suppressed by the proposed algorithm, which results in the enhancement of heading angle accuracy.

From the results shown in the table and figures, it is confirmed that the proposed measurements are sufficiently applicable for achieving enhanced heading accuracy.

B. EXPERIMENTAL RESULTS

To evaluate the performance of the proposed algorithm more practically, we performed several load tests and compared the performance of the proposed algorithm with those of the conventional GPS/INS. IMU and GPS were installed in a vehicle for the experiments. The IMU used in the experiment was SMI 130 from Bosch. The specifications of the experimental set are shown in Table 4. The STA8089FG GPS receiver from STMicroelectronics was used, and the velocity information provided by the Doppler shift was used. The performances of IMU and GPS used in the simulations and the experiments are the same as those used in Korean automotive industries.

For validating the algorithm, five different trajectories were tested for experiments. Fig. 7 and Fig. 8 show selected driving trajectories. For the trajectory 2, the experiments were

TABLE 4. Specification of SMI 130.

	Gyro	Accelerometer
Zero-point offset	$\pm 0.5°/s$	± 35 mg
Sensitivity error	$\pm 1\%$	$\pm 4\%$
RMS noise	$0.02°/s\sqrt{Hz}$	0.19 mg$\sqrt{Hz}$
Sampling rate	$20\ Hz$	$20\ Hz$

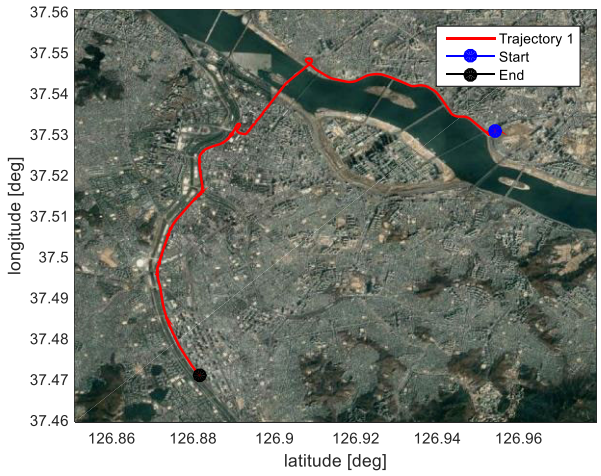

FIGURE 7. Experiment driving trajectory 1.

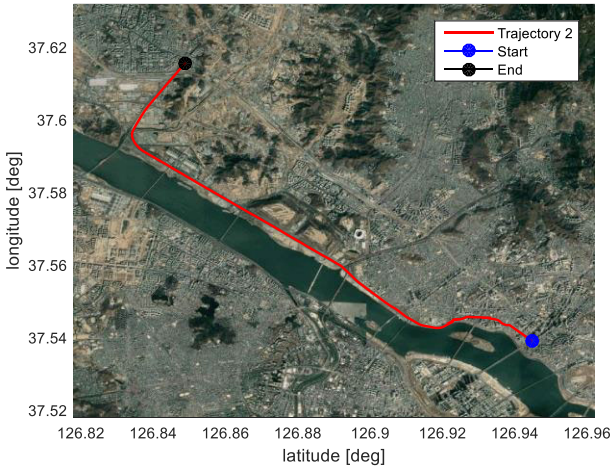

FIGURE 8. Experiment driving trajectory 2.

performed twice. The heading reference data are acquired from a map-based heading calculation.

Owing to the low performance of the IMU, it is impossible to estimate the velocity when only the GPS position is used as the measurement. Therefore, the performance evaluation is performed by comparing the proposed algorithm with the position+V_{dopp} case.

Table 5 shows the experimental results. The results show that the heading RMSEs are reduced by 20% on average when using the proposed algorithm. As there exist temperature drift, vibratory noise, misalignment, and other error sources, the overall heading accuracy is not good as that

TABLE 5. Experimental results of heading RMSE [deg].

Test Sets	Trajectories	Position + V_{dopp}	Proposed algorithm
1	Trajectory 1	1.9788	1.5257
2	Trajectory 2	1.7482	1.5510
3	Trajectory 2	1.3150	0.9347
4	Trajectory 3	1.5655	1.1614
5	Trajectory 4	2.0671	1.8769
6	Trajectory 5	1.4127	1.2809

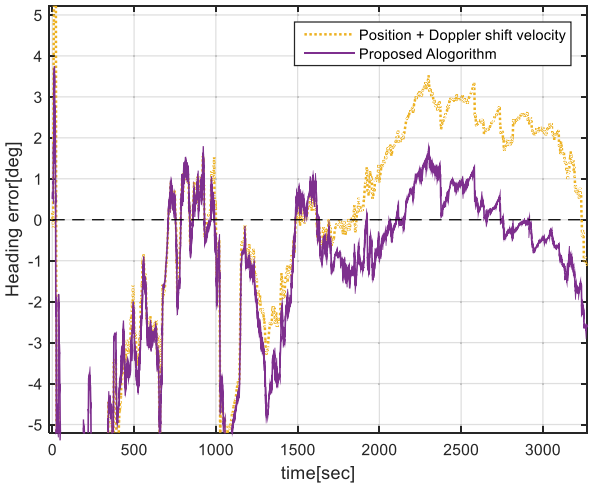

FIGURE 9. Experimental results for trajectory 1.

in the simulation cases. However, it can be concluded that the performance is enhanced significantly compared with the conventional algorithm.

Fig. 9 shows the heading error for the test set 1. The heading error when using the proposed algorithm is reduced by 20% in general. From 1250 seconds to 1400 seconds, small rotating movements are repeated, which can be considered as high dynamic situation. In this time period, the error of Position+ V_{dopp} becomes momentarily smaller than that of the proposed algorithm. But the error is suppressed soon after a vehicle moves with low dynamics. As a result, the proposed algorithm can be applied to the real vehicle navigation system contributing to the enhancement of heading accuracy.

V. CONCLUSION

In this paper, we proposed a heading accuracy enhancement algorithm that uses average velocity as a measurement. The proposed algorithm makes it possible to overcome the limitations of using the conventional GPS/INS integration algorithm, which uses instantaneous velocity as a measurement.

To validate the proposed algorithm, it is confirmed theoretically that the instantaneous velocity measurements can be substituted by the average velocity measurements in low dynamic situations. In addition, the advantage of the average velocity measurements is discussed. Based on a theoretical

approach, a new measurement is devised and analyzed, and the corresponding algorithm is proposed in this paper.

The performances of the proposed algorithm were verified through simulations and experiments. The estimation performance of the heading is improved significantly compared with that in other cases. In addition, the heading RMSE was reduced by approximately 20% in the simulations and experiments compared with other cases using the instantaneous velocity as a measurement. From these results, it is confirmed that the average velocity measurement is effective and relatively advantageous for the heading estimation because the average noise is relatively smaller than that in the instantaneous velocity and the baseline is longer.

Although the proposed algorithm can be applied to the existing GPS/INS integrated system easily, it still has some limitations. To apply the proposed algorithm in various dynamic situations, adaptation rules need to be developed. And the error model for the average velocity should be derived in the future. In addition, further studies on analyzing the characteristics of the proposed algorithm in various dynamic situations are required for applying the proposed algorithm to other systems such as drones or robotics.

REFERENCES

[1] J. W. Song and C. G. Park, "INS/GPS integrated smoothing algorithm for synthetic aperture radar motion compensation using an extended Kalman filter with a position damping loop," *Int. J. Aeronaut. Space Sci.*, vol. 18, no. 1, pp. 118–128, Mar. 2017.

[2] G. Hyslop, D. Gerth, and J. Kraemer, "GPS/INS integration on the stand-off land attack missile (SLAM)," in *Proc. IEEE Symp. Position Location Navigat. Decade Excellence Navigat. Sci.*, Mar. 1990, pp. 407–412.

[3] D.-B. Park, D.-H. Shin, S.-H. Oh, and H.-S. Kim, "Development of a GPS/INS system for precision GPS guided bombs," *IEEE Aerosp. Electron. Syst. Mag.*, vol. 27, no. 3, pp. 31–39, Mar. 2012.

[4] C. Zhang, C. Guo, and D. Zhang, "Ship navigation via GPS/IMU/LOG integration using adaptive fission particle filter," *Ocean Eng.*, vol. 156, pp. 435–445, May 2018.

[5] L. Arreola, A. Montes de Oca, A. Flores, J. Sanchez, and G. Flores, "Improvement in the UAV position estimation with low-cost GPS, INS and vision-based system: Application to a quadrotor UAV," in *Proc. Int. Conf. Unmanned Aircr. Syst. (ICUAS)*, Dallas, TX, USA, Jun. 2018, pp. 1248–1254.

[6] Y. Liu, X. Fan, C. Lv, J. Wu, L. Li, and D. Ding, "An innovative information fusion method with adaptive Kalman filter for integrated INS/GPS navigation of autonomous vehicles," *Mech. Syst. Signal Process.*, vol. 100, pp. 605–616, Feb. 2018.

[7] H. Xiong, Z. Mai, J. Tang, and F. He, "Robust GPS/INS/DVL navigation and positioning method using adaptive federated strong tracking filter based on weighted least square principle," *IEEE Access*, vol. 7, pp. 26168–26178, 2019.

[8] T. Suzuki, M. Kitamura, Y. Amano, and N. Kubo, "Autonomous navigation of a mobile robot based on GNSS/DR integration in outdoor environments," *J. Robot. Mechtron.*, vol. 26, no. 2, pp. 214–224, Apr. 2014.

[9] C.-S. Yoo and I.-K. Ahn, "Low cost GPS/INS sensor fusion system for UAV navigation," in *Proc. 22nd Digit. Avionics Syst. Conf. (DASC)*, Oct. 2003, p. 8. A. 1-8.1-9.

[10] T. Litman, *Autonomous Vehicle Implementation Predictions Implications for Transport Planning*. Victoria, BC, Canada: Victoria Transport Policy Institute, 2019, pp. 4–7.

[11] Z. Yu, Y. Hu, and J. Huang, "GPS/INS/Odometer/DR integrated navigation system aided with vehicular dynamic characteristics for autonomous vehicle application," *IFAC-PapersOnLine*, vol. 51, no. 31, pp. 936–942, 2018, doi: 10.1016/j.ifacol.2018.10.060.

[12] B.-H. Lee, J.-H. Song, J.-H. Im, S.-H. Im, M.-B. Heo, and G.-I. Jee, "GPS/DR error estimation for autonomous vehicle localization," *Sensors*, vol. 15, no. 8, pp. 20779–20798, Aug. 2015.

[13] M. Aftatah, A. Lahrech, and A. Abounada, "Fusion of GPS/INS/Odometer measurements for land vehicle navigation with GPS outage," in *Proc. 2nd Int. Conf. Cloud Comput. Technol. Appl. (CloudTech)*, Marrakesh, Morocco, May 2016, pp. 48–55.

[14] I. Abuhadrous, F. Nashashibi, and C. Laurgeau, "3-d land vehicle localization: A real-time multi-sensor data fusion approach using rtmaps," in *Proc. Int. Conf. Adv. Robot.*, Coimbra, Portugal, 2003, pp. 71–76.

[15] Y. Gao, S. Liu, M. Atia, and A. Noureldin, "INS/GPS/LiDAR integrated navigation system for urban and indoor environments using hybrid scan matching algorithm," *Sensors*, vol. 15, no. 9, pp. 23286–23302, Sep. 2015.

[16] A. Y. Hata and D. F. Wolf, "Feature detection for vehicle localization in urban environments using a multilayer LIDAR," *IEEE Trans. Intell. Transp. Syst.*, vol. 17, no. 2, pp. 420–429, Feb. 2016.

[17] L. Wang, Y. Zhang, and J. Wang, "Map-based localization method for autonomous vehicles using 3D-LIDAR," *IFAC-PapersOnLine*, vol. 50, no. 1, pp. 276–281, Jul. 2017, doi: 10.1016/j.ifacol.2017.08.046.

[18] Y. Choe, C. G. Park, and J. W. Song, "Importance sampling Kalman filter for urban canyon navigation," in *Proc. IEEE/ION Position, Location Navigat. Symp. (PLANS)*, Monterey, CA, USA, Apr. 2018, pp. 1264–1269.

[19] X. Qu, B. Soheilian, and N. Paparoditis, "Vehicle localization using mono-camera and geo-referenced traffic signs," in *Proc. IEEE Intell. Vehicles Symp. (IV)*, Seoul, South Korea, Jun. 2015, pp. 605–610.

[20] D. Gruyer, R. Belaroussi, and M. Revilloud, "Accurate lateral positioning from map data and road marking detection," *Expert Syst. Appl.*, vol. 43, pp. 1–8, Jan. 2016.

[21] N. Sairam, S. Nagarajan, and S. Ornitz, "Development of mobile mapping system for 3D road asset inventory," *Sensors*, vol. 16, no. 3, p. 367, Mar. 2016.

[22] C. Shen, Z. Bai, H. Cao, K. Xu, C. Wang, H. Zhang, D. Wang, J. Tang, and J. Liu, "Optical flow Sensor/INS/Magnetometer integrated navigation system for MAV in GPS-denied environment," *J. Sensors*, vol. 2016, pp. 1–10, 2016, doi: 10.1155/2016/6105803.

[23] H. Pang, M. Pan, C. Wan, J. Chen, X. Zhu, and F. Luo, "Integrated compensation of magnetometer array magnetic distortion field and improvement of magnetic object localization," *IEEE Trans. Geosci. Remote Sens.*, vol. 52, no. 9, pp. 5670–5676, Sep. 2014.

[24] J. Song and C. Park, "Enhanced pedestrian navigation based on course angle error estimation using cascaded Kalman filters," *Sensors*, vol. 18, no. 4, p. 1281, Apr. 2018.

[25] Z. Wu, M. Yao, H. Ma, and W. Jia, "Improving accuracy of the vehicle attitude estimation for low-cost INS/GPS integration aided by the GPS-measured course angle," *IEEE Trans. Intell. Transp. Syst.*, vol. 14, no. 2, pp. 553–564, Jun. 2013.

[26] S. Gaglione and M. Petovello, "How does a GNSS receiver estimate velocity?" *Inside GNSS*, vol. 10, no. 2, pp. 38–41, Mar. 2015.

[27] P. Misra and P. Enge, *Global Positioning System Signals, Measurements and Performance*, 2nd ed. Lincoln, MA, USA: Ganga-Jamuna Press, 2006, ch. 6, pp. 199–219.

[28] B. Hofmann-Wellenhof, H. Lichtenegger, and J. Collins, *Global Positioning System: Theory and Practice*, 5th ed. New York, NY, USA: Springer, 2013, ch. 8, pp. 181–187.

[29] D. M. Bevly, J. C. Gerdes, C. Wilson, and G. Zhang, "The use of GPS based velocity measurements for improved vehicle state estimation," in *Proc. Amer. Control Conf. (ACC)*, Chicago, IL, USA, vol. 4, 2000, pp. 2538–2542.

[30] S. Sen, S. Chakraborty, and A. Sutradhar, "Estimation of tire slip-angles for vehicle stability control using Kalman filtering approach," in *Proc. Int. Conf. Energy, Power Environ., Towards Sustain. Growth (ICEPE)*, Shillong, India, Jun. 2015, pp. 1–6.

[31] P. M. G. Silson, "Coarse alignment of a ship's strapdown inertial attitude reference system using velocity loci," *IEEE Trans. Instrum. Meas.*, vol. 60, no. 6, pp. 1930–1941, Jun. 2011.

[32] D. Titterton, J. L. Weston, and J. Weston, *Strapdown Inertial Navigation Technology*, 2nd ed. Edison, NJ, USA: IET, 2004, ch. 12, pp. 342–345.

[33] P. D. Groves, *Principles of GNSS, Inertial, and Multisensor Integrated Navigation Systems*, 2nd ed. Norwood, MA, USA: Artech House, 2008, ch. 14, pp. 560–589.

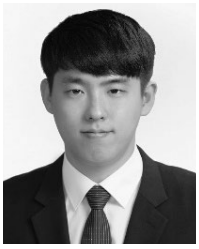

MIN JUN CHOI received the B.S. degree in robotics engineering from Hoseo University, in 2018. He is currently a Graduate Student with the Department of Software Convergences, Sejong University, Seoul, South Korea. His research interests include GPS/INS integration, SDINS, unmanned vehicle navigation, autonomous navigation systems.

YONG HUN KIM received the B.S. degree in robotics engineering from Hoseo University, in 2018. He is currently a Graduate Student with the Department of Software Convergences, Sejong University, Seoul, South Korea. His research interests include pedestrian navigation, indoor navigation, personal navigation systems, and GPS/INS.

EUNG JU KIM received the B.S. degree in robotics engineering from Hoseo University, in 2018. From 2016 to 2018, he was a CEO with Yewon Robotics. He is currently a Graduate Student with the Department of Software Convergences, Sejong University, Seoul, South Korea. His research interests include sensor fusion, FDI algorithm, navigation systems, GPS/INS integration, and optimal control.

JIN WOO SONG (Member, IEEE) received the B.S. and M.S. degrees in control and instrumentation engineering and the Ph.D. degree in electrical, electronic, and computer engineering from Seoul National University, Seoul, South Korea, in 1995, 1997, and 2002, respectively. From 2003 to 2014, he was a CTO with Microinfinity Company, Ltd. Since 2014, he has been a Research Professor of the BK21Plus Transformative Training Program for Creative Mechanical and Aerospace Engineers, Department of Mechanical and Aerospace Engineering, Seoul National University. From 2016 to 2017, he was an Assistant Professor with the Department of Robotics Engineering, Hoseo University, Asan, South Korea. He is currently an Assistant Professor with the School of Intelligent Mechatronics Engineering, Sejong University, Seoul. His research interests include GPS/INS integration, robust and optimal control, MEMS inertial sensors and systems, indoor navigation, and robot localization.